JOURNAL OF SOLID STATE CHEMISTRY **124,** 230–237 (1996)
ARTICLE NO. 0231

Oxygen Diffusion in $LaMnO_3$ and $LaCoO_3$ Perovskite-Type Oxides: A Molecular Dynamics Study

M. S. Islam,*,[1] M. Cherry,*,† and C. R. A. Catlow†

*Department of Chemistry, University of Surrey, Guildford GU2 5XH, United Kingdom; and
†Davy-Faraday Laboratories, The Royal Institution, London W1X 4BS, United Kingdom

Received January 18, 1996; accepted April 1, 1996

Oxygen ion diffusion in the $La_{1-x}Sr_xMnO_3$ and $La_{1-x}Sr_xCoO_3$ materials is investigated using Molecular Dynamics (MD) techniques. The results presented give both quantitative and qualitative information on the oxygen diffusion coefficients over a broad temperature range and on the structure of the crystal lattice. The pair distribution functions indicate significant disorder on the mobile oxygen sublattice especially at elevated temperatures. The simulations are used to construct Arrhenius plots of oxygen diffusion in the doped perovskites, from which we find good agreement between the calculated and experimental activation energies. In addition, useful information on the atomistic mechanisms for oxygen migration has been obtained from the analysis of ion trajectories.

1. INTRODUCTION

The $LaMO_3$ perovskite-structured oxides that display high oxygen ion mobility have been extensively investigated (1–12), much of this work being motivated by the potential use of these materials in solid oxide fuel cells and as effective heterogeneous catalysts. These technological applications stimulate interest in improving the fundamental understanding of the oxygen transport properties of the materials which depends crucially on a full characterization of the structure and dynamics of the mobile sublattice. It is also well known that the partial substitution of La by acceptor dopants enhances the ionic conductivity by increasing the oxygen vacancy concentration especially at low oxygen activity. However, despite several reports of the electrical conductivity of these perovskite-structured materials (1, 5, 7, 10), there are far fewer studies of the oxygen diffusion parameters and limited information on mechanistic features at the atomic level.

We have already obtained via computational methods valuable information on some of the factors controlling oxygen (and proton) transport in $LaMO_3$ (where M = Cr, Mn, Fe, Co), as well as on the effects of dopant substitution and hole formation (13, 14). The present study will amplify this knowledge by a detailed investigation of oxygen diffusion using Molecular Dynamics (MD) techniques which include thermal effects explicitly; these computational techniques have been successfully applied to a variety of fast-ion conductors such as Na β''-Al_2O_3 (15) and CaF_2 (16, 17), but have not been widely applied to perovskite-type oxides. In the present work we have focused attention on two representative systems, namely $La_{1-x}Sr_xMnO_3$ and $La_{1-x}Sr_xCoO_3$, for which there is experimental diffusion data for direct comparison.

2. SIMULATION METHODS

The MD technique consists of an explicit dynamical simulation of the ensemble of particles for which Newton's equations of motion are solved. Repetition of the integration algorithm yields a detailed picture of the evolution of the system as a function of time. Detailed reviews of the MD technique have been given previously (18) and will only be outlined here.

The interatomic forces of the polar solid are represented by effective pair-potentials of the Buckingham form

$$V_{ij}(r) = -Z_iZ_je^2/r + A_{ij}\exp(-r/\rho) - C_{ij}/r^6, \qquad [1]$$

which includes the long-range Coulomb term and a short-range function to model overlap-repulsion and dispersion forces. For $LaMnO_3$ and $LaCoO_3$, the potential parameters were derived simultaneously by empirical fitting to observed crystal properties; this procedure resulted in a common set of interatomic potentials which are listed in Table 1. Previous studies (13, 14) have shown that these models reproduce adequately the crystal properties of the perovskite oxides.

As with most MD studies, the shell model to treat ionic polarization has not been included owing to the considerable increase in computer time required for such simulations. In the case of the cations this should lead to negligible

[1] To whom correspondence should be addressed. E-mail: m.islam@surrey.ac.uk.

0022-4596/96 $18.00

TABLE 1
Interatomic Potentials for $LaMnO_3$ and $LaCoO_3$

Interaction	A(eV)	ρ(Å)	C(eV/Å^6)
$La^{3+} \cdots O^{2-}$	1516.3	0.3525	0.0
$Mn^{3+} \cdots O^{2-}$	1235.9	0.3281	0.0
$Co^{3+} \cdots O^{2-}$	636.4	0.3675	0.0
$Sr^{2+} \cdots O^{2-}$	774.2	0.3538	0.0
$O^{2-} \cdots O^{2-}$	22764.3	0.1490	43.0

errors, but the polarizability of the O^{2-} ion will be significant and is expected to be the major shortcoming of the potential model. Nevertheless, the potential parameters used in this study were derived to produce static dielectric constants (listed in Table 2) that are comparable to the values obtained from shell-model potentials employed in our static lattice simulations of these oxides (13). It is worth noting that a recent shell model MD study of CaF_2 found that the explicit inclusion of polarizability had little effect on the structure and diffusion dynamics in the superionic state (17).

The MD simulations reported here were performed using the DLPOLY code (19) with a simulation box comprising 2560 ions (i.e., $8 \times 8 \times 8$ perovskite unit cells) to which periodic boundary conditions were applied; the ensemble used imposes the conditions of constant temperature and pressure (NPT). The calculations were run using a time step (δt) of 10^{-15} s and for a total period of 50 ps including initial equilibration (of 4 ps). It is worth remarking that we are employing a longer time scale than the majority of previous MD simulations of polar solids. The doped systems $La_{1-x}Sr_xMnO_3$ and $La_{1-x}Sr_xCoO_3$ were modeled by the partial substitution of La by Sr (introduced at random) and the corresponding removal of oxygen ions as charge-compensating vacancy defects.

3. RESULTS AND DISCUSSION

3.1. Structural Properties

Structural information can be extracted from MD studies via the pair correlation function (PCF) $g(r)$ which is given by

$$g_{ij}(r) = \langle n_{ij}(r) \rangle / 4\pi r^2 (n_i n_j)^{1/2}, \qquad [2]$$

where i, j are ion types; $\langle n_{ij}(r) \rangle$ is the ensemble average of the number of species of type j in a radial shell of $r \rightarrow r + dr$ with a species of type i at the center; n_i is the bulk density of ion type i. The PCF provides an insight into the long-range (dis)order of the crystal lattice.

TABLE 2
Calculated Crystal Properties of $LaMnO_3$ and $LaCoO_3$

Property	$LaMnO_3$	$LaCoO_3$
Lattice parameter (Å)	3.904	3.820
Lattice energy (eV)	−139.12	−139.74
Static dielectric constant (ε_0)	56.17	22.95

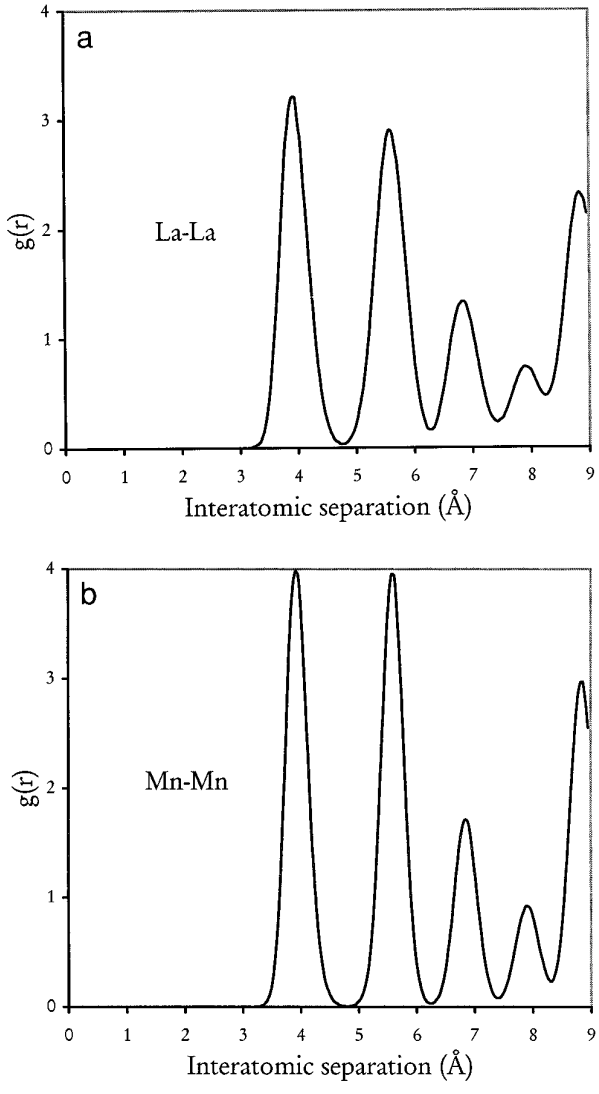

FIG. 1. Pair correlation functions for cations in $La_{0.8}Sr_{0.2}MnO_3$ at 2000 K; (a) La–La, (b) Mn–Mn.

We first consider the cation pair correlation functions for the doped systems $La_{0.8}Sr_{0.2}MnO_3$ and $La_{0.8}Sr_{0.2}CoO_3$, which are shown in Figs. 1 and 2, respectively. These plots reveal a series of well-defined peaks corresponding to successive nearest-neighbor distances, which is normal behavior for an ordered solid. By contrast, the O–O pair functions for the doped systems (presented in Fig. 3) show weak, diffuse structure for separations larger than nearest-neighbor; this points to the loss of long-range order on the mobile oxygen sublattice. Figure 3 also reveals that as the

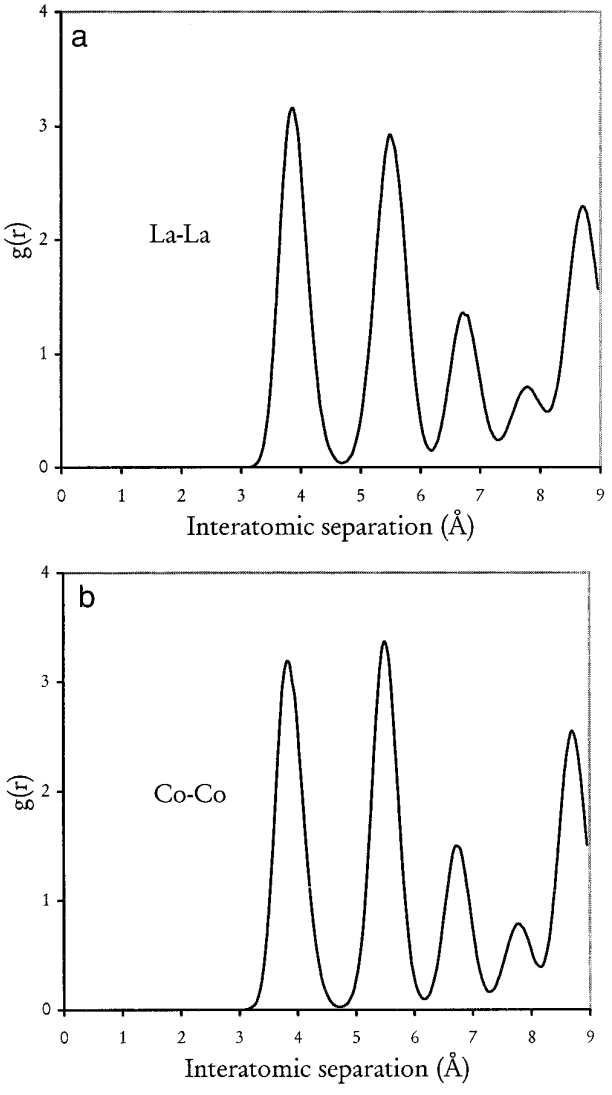

FIG. 2. Pair correlation functions for cations in $La_{0.8}Sr_{0.2}CoO_3$ at 2000 K; (a) La–La, (b) Co–Co.

temperature increases from 800 to 2000 K the first peak decreases in height, while the general profile broadens indicating a greater degree of disorder at higher temperatures. It is interesting to note that these O–O pair functions show diffuse behavior that is more typical of the PCFs of the mobile ions in superionic conductors. This suggests that, when not directly involved in the diffusion process, the oxygen ion exhibits significant deviation from the regular site, a point to which we return below.

3.2. Diffusion Coefficient

Atomic transport properties are extracted from the simulations using the time-dependent mean square displacements (MSD), which are defined in the usual way,

$$\langle r^2(t)\rangle = 1/N_i \sum_{i=1} \{[x_i(t) - x_i(0)]^2 + [y_i(t) - y_i(0)]^2 + [z_i(t) - z_i(0)]^2\}, \quad [3]$$

where $x_i(t)$ is the x coordinate of ion i at time t. The MSDs for all the ions in the two doped systems $La_{0.8}Sr_{0.2}MnO_3$ and $La_{0.8}Sr_{0.2}CoO_3$ at 2000K are presented in Fig. 4. They clearly show that the MSD of the cations tends rapidly to a constant value following equilibration and confirms that there is no cation diffusion in the perovskite oxides. However, the MSD for the oxygen ions increases with time indicating significant ion diffusion; this type of behavior is found in simulations of other solid electrolytes such as Y/ZrO_2 (20). We note that the basic features of the plots are very similar for all the temperatures considered be-

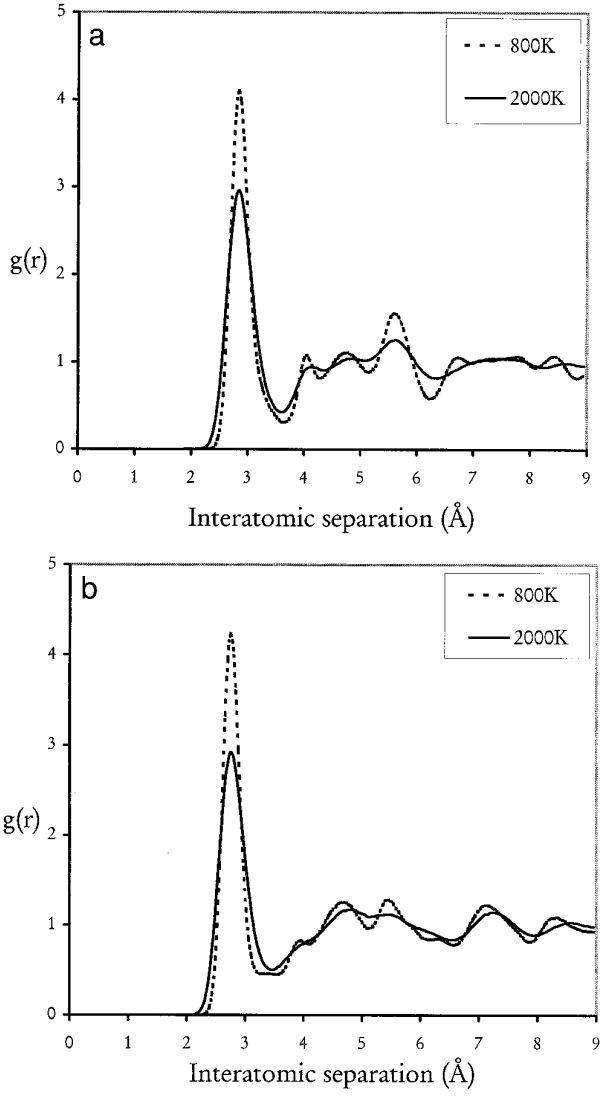

FIG. 3. Pair correlation functions for O–O at 800 and 2000 K; (a) $La_{0.8}Sr_{0.2}MnO_3$, (b) $La_{0.8}Sr_{0.2}CoO_3$.

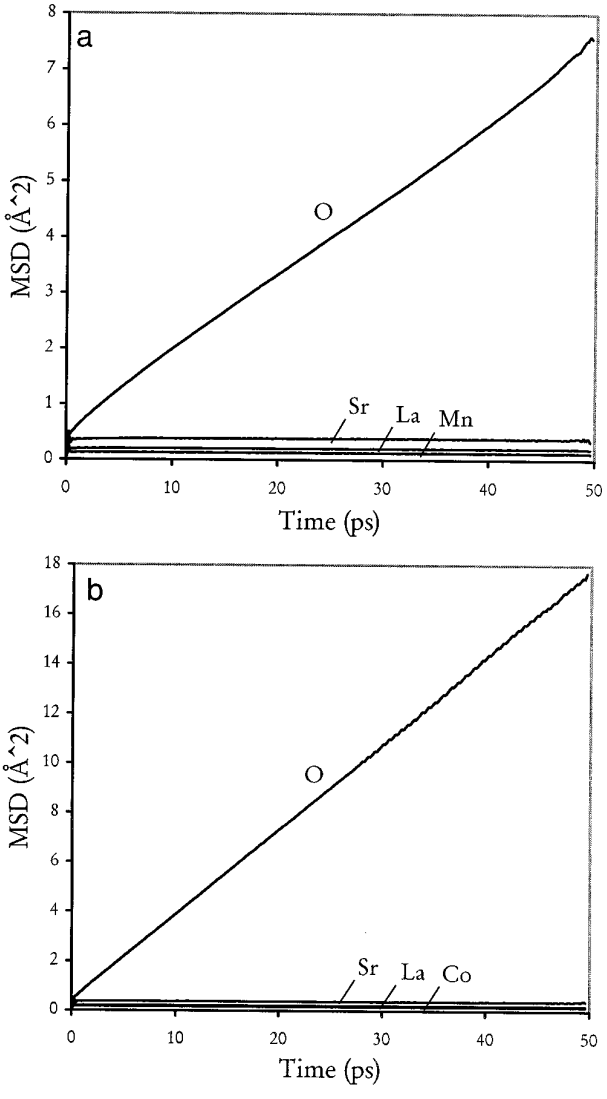

FIG. 4. Mean square displacements of all ions at 2000 K; (a) $La_{0.8}Sr_{0.2}MnO_3$, (b) $La_{0.8}Sr_{0.2}CoO_3$.

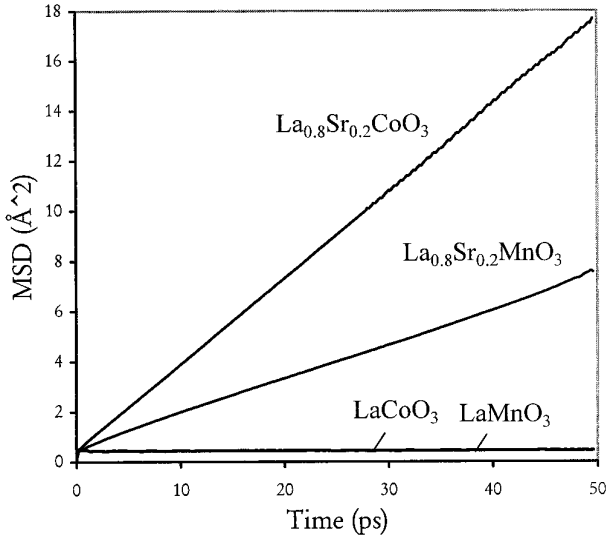

FIG. 5. Mean square displacements of oxygen ions in both undoped and doped perovskites at 2000 K.

tween 800 and 2000 K. In Fig. 5 we focus on the MSD of oxygen ions in both the doped and undoped materials, which clearly demonstrates that the functions are constant with time in undoped $LaMnO_3$ and $LaCoO_3$. This indicates that no detectable oxygen diffusion is exhibited in the pure stoichiometric materials and that acceptor doping is crucial to enhancing ionic conductivity.

The diffusion coefficient (D_i) can be obtained from the gradient of the plot of MSD against time according to the relation

$$\langle r^2(t)\rangle = 6D_i t + B_i, \qquad [4]$$

where B_i is the thermal factor arising from atomic vibrations. The calculated oxygen diffusion coefficients for both systems are given in Table 3 and presented in the form of Arrhenius plots (ln D versus $1/T$) in Fig. 6, on which we also indicate experimentally determined values.

The results indicate three main points. First, we have been able to calculate values of the oxygen diffusion coefficient (D_0) over a broad range of about two orders of magnitude, which is significantly wider than the experimental data. Second, the diffusion coefficients for the manganate systems are in good agreement with the available

TABLE 3
Calculated Oxygen Diffusion Coefficients for (a) $La_{1-x}Sr_xMnO_3$ and (b) $La_{1-x}Sr_xCoO_3$

(a)	D_0(cm²/s)	
T(K)	$x = 0.2$	$x = 0.5$
800	1.51×10^{-8}	5.32×10^{-8}
1000	6.23×10^{-8}	1.48×10^{-7}
1200	1.08×10^{-7}	5.52×10^{-7}
1500	4.21×10^{-7}	9.17×10^{-7}
2000	3.41×10^{-6}	9.25×10^{-6}
(b)	D_0(cm²/s)	
T(K)	$x = 0.1$	$x = 0.2$
800	1.47×10^{-7}	1.92×10^{-7}
1000	3.02×10^{-7}	4.05×10^{-7}
1200	4.83×10^{-7}	1.12×10^{-6}
1500	2.03×10^{-7}	3.65×10^{-6}
2000	3.61×10^{-6}	1.25×10^{-5}

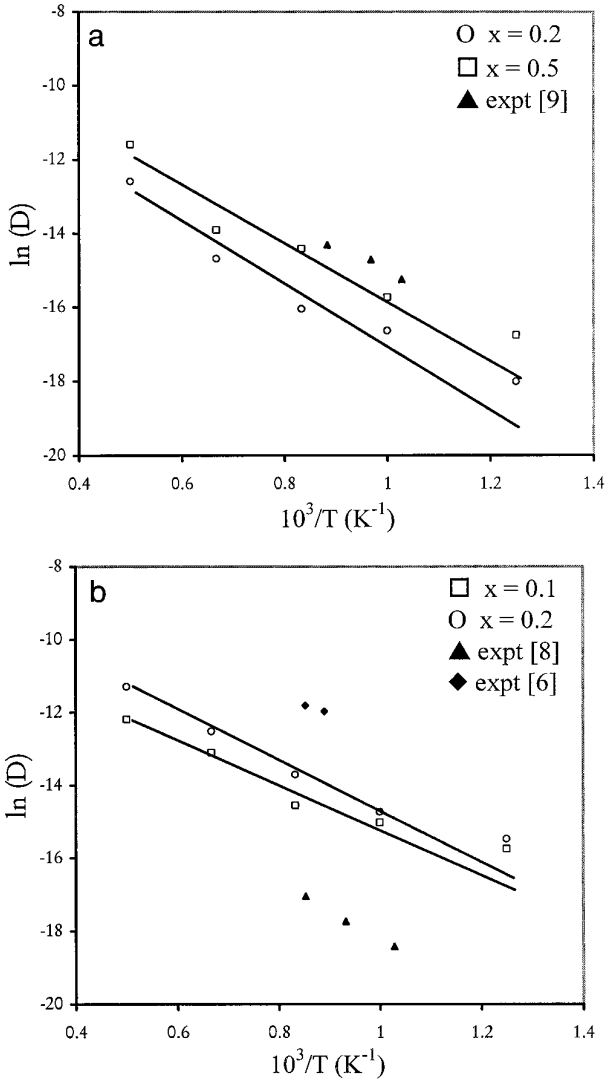

FIG. 6. Arrhenius plots for oxygen diffusion; (a) $La_{1-x}Sr_xMnO_3$, (b) $La_{1-x}Sr_xCoO_3$.

chemical diffusion coefficients of Belzner *et al.* (9). However, the calculated results for the cobaltate material appear to be somewhat greater than the oxygen self diffusion coefficients obtained from isotope exchange experiments (8), although the slopes of the Arrhenius plots and hence our activation energies compare well with their observed values (Table 4). We also include in Fig. 6 chemical diffusion coefficients from Alcock *et al.* (6) which are clearly greater than both sets of values and indicate that direct comparison is not straightforward. Finally, the simulations suggest a higher oxygen diffusivity in the cobalt-based materials than that in the manganates, with D_0 increasing with greater Sr doping owing to a corresponding increase in the vacancy concentration.

Such rapid oxygen transport in these perovskite-type

TABLE 4
Calculated and Experimental Activation Energies for Oxygen Ion Migration

System	Activation energy (eV)	
	Calc.	Expt.
$La_{0.8}Sr_{0.2}MnO_3$	0.70	0.73[a]
$La_{0.5}Sr_{0.5}MnO_3$	0.67	—
$La_{0.9}Sr_{0.1}CoO_3$	0.51	—
$La_{0.8}Sr_{0.2}CoO_3$	0.59	0.62 ± 0.2[b]; 0.78 ± 0.22[c]

[a] Belzner *et al.* (9).
[b] Carter *et al.* (8).
[c] Ishigaki *et al.* (12).

oxides is a vital characteristic for their application in solid oxide fuel cells, oxidation catalysis, and gas separation. However, we recognize that $LaMO_3$ materials show complex behavior when acceptor doped because of the ability of the M cation to change valence which may lead to compensation by a mixture of oxygen vacancies and holes (8, 13). This is an area that warrants further investigation.

From the slopes of the Arrhenius plots (Fig. 6) we may derive the activation energy for oxygen migration; these are listed in Table 4 in which observed values are also included. The good measure of agreement between the calculated and experimental activation energies is most encouraging and provides support that the MD simulation is indeed a realistic representation of the microscopic process of diffusion. The slight curvature in the data points in Fig. 6 is largely due to the improved statistics of the simulations for the much higher diffusion coefficients at elevated temperatures. We have therefore neglected the point from the 800 K simulation, although the deviation at lower temperatures are within the uncertainties owing to the statistical errors of the data.

The dopant concentration, which directly determines the population of mobile oxygen vacancies, has a direct effect upon the activation energy. For the manganate

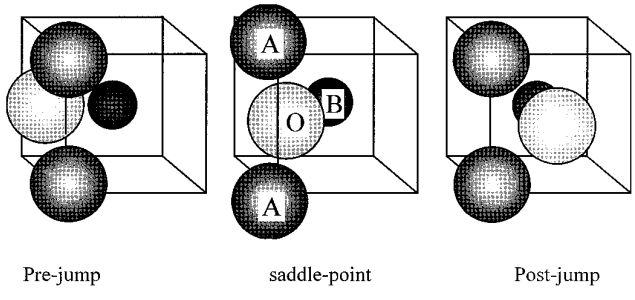

FIG. 7. Schematic representation of the migration of a single oxygen ion along the edge of the BO_6 octahedron (only three cations are shown for clarity).

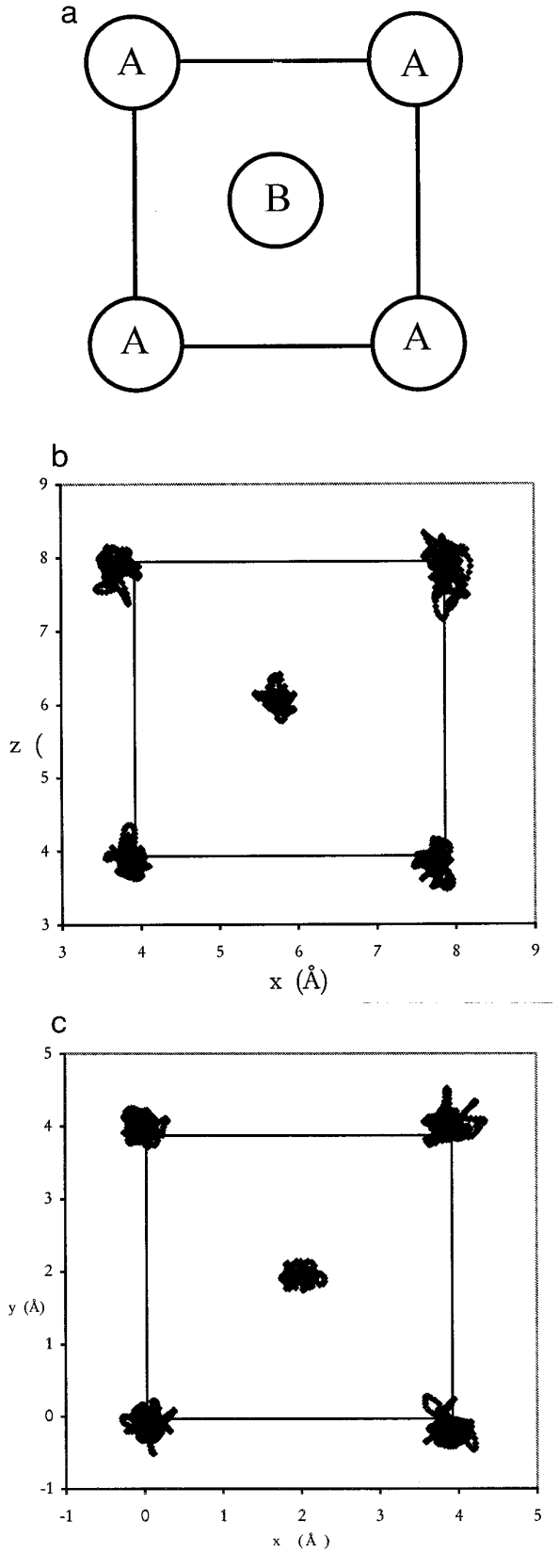

system, we find that an increase in the dopant concentration leads to a higher rate of diffusion and a small change in the activation energy. However, a significant increase in the activation energy at the higher dopant level is found in $La_{1-x}Sr_xCoO_3$ (Table 4). This difference between the two cobaltate compositions is likely to be attributed to dopant-vacancy interactions and the formation of defect clusters. Indeed, it is well known that for the fluorite-structured ion conductors (e.g., rare-earth doped CeO_2) the ionic conductivity is dependent upon the extent of defect clustering which adds a binding (or association) term to the Arrhenius energy (21). In this context it is interesting to note that our previous lattice simulations of $LaMO_3$ (M = Cr, Mn, Fe, Co) (13) found that the $(Sr'_{La}V^{\cdot\cdot}_0)$ pair cluster is bound only in the $LaCoO_3$ material with a binding energy of -0.2 eV. This result is consistent with the difference in calculated activation energy between the two cobaltate systems in the present study.

3.3. Migration Mechanism

A major thrust of basic transport studies has been the determination of the atomistic mechanisms controlling bulk transport phenomena. Indeed, the unravelling of mechanistic detail at the microscopic level, which can be difficult from purely experimental studies, is a powerful feature of the MD technique.

Analysis of the ion trajectories, with the aid of the INSIGHT graphics code (22), confirms the extensive motion of the oxygen sublattice in these perovskite oxides. Figure 7 shows a schematic representation of the simulated trajectory of a single oxygen ion; this reveals that anion migration takes place by conventional hops of oxygen ions directly into adjacent vacant sites with no evidence of correlated motion. The pathway is along the edge of the BO_6 octahedron, passing through a ''saddle-point'' position defined by the center of a triangle comprised of two A site (La) ions and one B site (Mn or Co) ion. From our analysis of the saddle-point configuration, we find significant outward relaxation of the cations away from the mobile oxygen ion which probably reduces any repulsive overlap interactions. We should note that the predicted migration pathway and relaxation effects are in accord with our previous static lattice studies in which we also found a strong correlation between the calculated activation energy and the perovskite tolerance factor. (13)

To gain further insight into the migration mechanism we have obtained ''trajectory plots'' which reveal the evo-

FIG. 8. Trajectory plot of cations; (a) schematic of cation positions (projection into unit cell face relating to two layers parallel to (100), (b) $La_{0.8}Sr_{0.2}MnO_3$, (c) $La_{0.8}Sr_{0.2}CoO_3$.

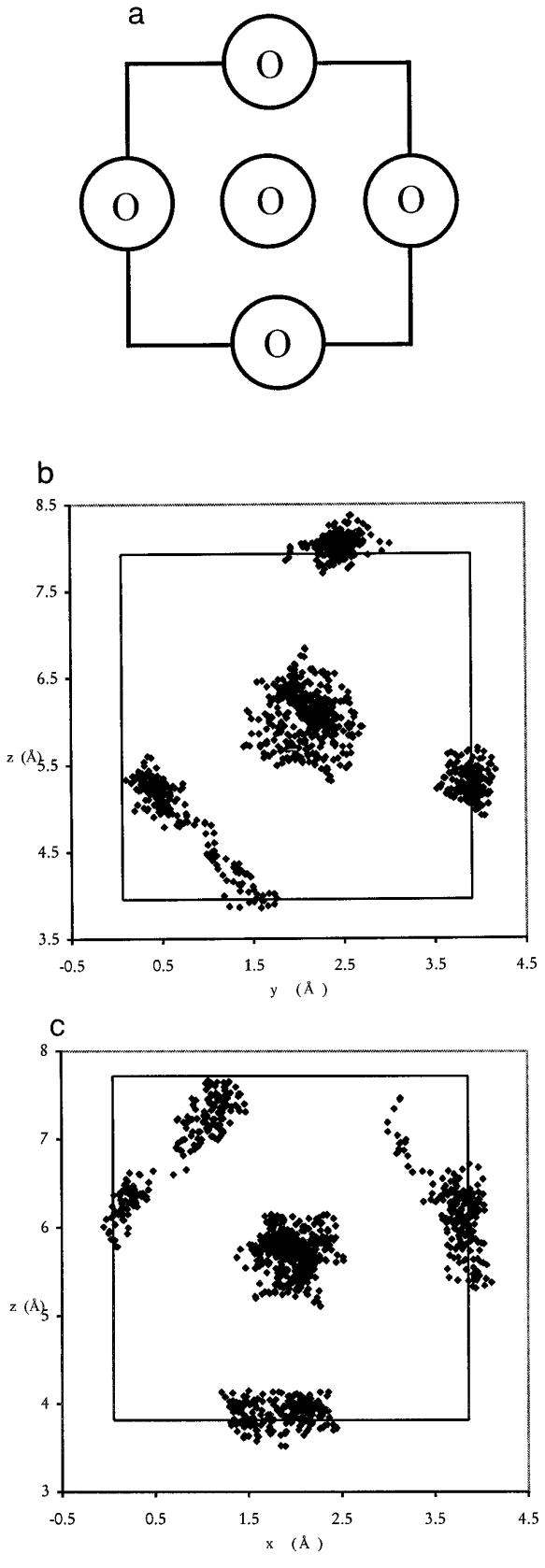

lution of the displacement of the ions (Figs. 8 and 9). It should be noted that these plots relate to a projection into the face of one unit cell (i.e., the figures relate to ions in two layers parallel to the (100) plane). Figure 8 clearly indicates small vibrations of the cations about their lattice sites with no evidence of ion diffusion, which is typical behavior for an ordered solid. In contrast, Fig. 9 shows a more diffuse distribution on the oxygen sublattice for $La_{0.8}Sr_{0.2}MnO_3$ and $La_{0.8}Sr_{0.2}CoO_3$ indicating significant ion motion; the diffusion of oxygen is illustrated by the spread of points between adjacent lattice sites along the octahedron edge. It is also apparent that the oxygen vacancies induce a strong relaxation of neighboring anions causing a distortion of the octahedra, a feature also implied by the PCF results.

4. CONCLUSION

Molecular Dynamics (MD) techniques have been used to investigate the structural and transport properties of oxygen diffusion in $La_{1-x}Sr_xMnO_3$ and $La_{1-x}Sr_xCoO_3$. Our discussion has drawn attention to four main points:

(i) The pair correlation functions indicate considerable disorder on the mobile oxygen sublattice, more typical of a superionic conductor. The degree of disorder increases at higher temperatures associated with enhanced oxygen diffusion.

(ii) Oxygen diffusion coefficients have been calculated over a wider temperature range than the available experimental data and indicate rapid oxygen transport. We find no sign of ion diffusion in the undoped stoichiometric oxides and confirm that acceptor doping is crucial to high ionic conductivity (and high oxygen fluxes).

(iii) The calculated activation energies, derived from our Arrhenius plots, are higher in the manganates than in the cobaltates and are consistent with observed values.

(iv) Analysis of the atom trajectories points to a conventional hopping mechanism along the BO_6 octahedron edge for oxygen vacancy migration, with no evidence of correlated motion. We find significant outward relaxation of the cations away from the migrating oxygen ion at the saddle-point position.

Further studies will include doped systems with a mixture of vacancy and hole compensation.

ACKNOWLEDGMENTS

M.C. is supported by an EPSRC/CASE studentship with British Petroleum. We thank S. Ramdas, J. A. Kilner, and C. Pereira for helpful

FIG. 9. Trajectory plot of oxygen ions; (a) schematic of anion positions (projection into unit cell face relating to two layers parallel to (100), (b) $La_{0.8}Sr_{0.2}MnO_3$, (c) $La_{0.8}Sr_{0.2}CoO_3$.

discussions. The DLPOLY code was provided by W. Smith at the Daresbury Laboratory.

REFERENCES

1. L-W. Tai, M. M. Nasrallah, and H. U. Anderson, *J. Solid State Chem.* **118,** 117 (1995).
2. P. D. Petrolekas and I. S. Metcalfe, *J. Catal.* **152,** 147 (1995).
3. J. Ranlov, N. Bonanos, F. W. Poulsen, and M. Mogensen, *Solid State Phenom.* **39–40,** 219 (1994).
4. P. Salomonsson, T. Griffin, and B. Kasemo, *Appl. Catal.* **104,** 175 (1993).
5. T. Inoue, J. Kamimae, M. Ueda, K. Eguchi, and H. Arai, *J. Mater. Chem.* **3,** 751 (1993).
6. H. Kruidhof, H. J. M. Bouwmeester, R. H. E. van Doorn, and A. J. Burgraaf, *Solid State Ionics* **63–65,** 816 (1993).
7. J. Mizusaki, *Solid State Ionics* **52,** 79 (1992).
8. S. Carter, A. Selcuk, R. J. Chater, J. Kajda, J. A. Kilner, and B. C. H. Steele, *Solid State Ionics* **53–56,** 597 (1992).
9. A. Belzner, T. M. Gur, and R. A. Huggins, *Solid State Ionics* **57,** 327 (1992).
10. C. B. Alcock, R. C. Doshi, and Y. Shen, *Solid State Ionics* **51,** 281 (1992).
11. R. L. Cook and A. F. Sammells, *Solid State Ionics* **45,** 311 (1991).
12. T. Ishigaki, S. Yamauchi, K. Kishio, J. Mizusaki, and K. Fueki, *J. Solid State Chem.* **73,** 179 (1988).
13. M. Cherry, M. S. Islam, and C. R. A. Catlow, *J. Solid State Chem.* **118,** 125 (1995); M. S. Islam, M. Cherry, and L. J. Winch, *J. Chem. Soc., Faraday Trans.* **92,** 479 (1996).
14. M. Cherry, M. S. Islam, J. D. Gale, and C. R. A. Catlow, *J. Phys. Chem.* **99,** 14614 (1995).
15. W. Smith and M. J. Gillan, *J. Phys.: Condens. Matter* **4,** 3215 (1992).
16. G. A. Evangelakis and V. Pontikis, *Phys. Rev. B* **43,** 3180 (1991).
17. P. J. D. Lindan and M. J. Gillan, *J. Phys.: Condens. Matter* **5,** 1019 (1993).
18. M. P. Allen and D. J. Tildesley, ''Computer Simulation of Liquids.'' Oxford University Press, Oxford, 1987.
19. T. R. Forester and W. Smith, DLPOLY code, Daresbury Laboratory, UK, 1993.
20. X. Li and B. Hafskjold, *J. Phys.: Condens. Matter* **7,** 1255 (1995).
21. J. A. Kilner and R. J. Brook, *Solid State Ionics* **6,** 237 (1982).
22. INSIGHT II, Biosym Technologies, San Diego.